Hindawi
Advances in Materials Science and Engineering
Volume 2020, Article ID 3569125, 13 pages
https://doi.org/10.1155/2020/3569125

Research Article

Study on the Preparation of Biohydrocarbon Fuel by Catalytic Hydrogenation of *Swida wilsoniana* Pyrolysis Products

Aihua Zhang,[1,2] Juan Tang,[1] Jilie Lie,[1] Yidan He,[1] and Zhihong Xiao [2]

[1]*Central South University of Forestry and Technology, Changsha 410004, China*
[2]*Hunan Academy of Forestry, Changsha 410004, China*

Correspondence should be addressed to Zhihong Xiao; xzhh1015@163.com

Received 18 May 2020; Revised 19 July 2020; Accepted 30 July 2020; Published 17 September 2020

Academic Editor: Marco Cannas

Copyright © 2020 Aihua Zhang et al. This is an open access article distributed under the Creative Commons Attribution License, which permits unrestricted use, distribution, and reproduction in any medium, provided the original work is properly cited.

The Ni-ZSM-5 catalyst, under four different factors of *Swida wilsoniana* pyrolysis products of catalytic hydrogenation, GC-MS, FI-IR, and elemental analyzers, was used to identify the elements, carbon chain distribution, and composition of the products. The effects of reaction temperature, reaction pressure, and catalyst hydrogenation level on the conversion rate were investigated. The reaction pressure and the amount of catalyst are the main factors that affect the conversion of the pyrolysis products into biofuels. Using 1.05 wt.% Ni-ZSM-5 catalyst, the highest conversion rate was 98.10% at 173°C and 2.00 MPa. The results show that *Swida wilsoniana*-decomposed products can be converted to high-quality biofuels by catalytic hydrogenation of Ni-ZSM-5 and can be used as an alternative energy source.

1. Introduction

The development of contemporary human civilization and economy is based on fossil energy. However, the excessive development and use of human resources and the depletion of fossil energy reserves cause a series of problems such as the greenhouse effect, atmospheric pollution, and water pollution [1–3]. In this context, energy security is currently a hot spot of global concern [4]. Biomass energy has the advantages of reproducibility, recyclability, and no harm to the environment. Biomass energy is known as green energy, and it became one of the important contents of the energy strategies of countries in the world today [5, 6]. Researchers have paid close attention to the production of clean biohydrocarbon fuels from vegetable oils recently. Because of the versatility of biohydrocarbon fuels, it can be used as a substitute for fuel or as an additive for fossil fuel, and it also provides solutions for the future energy and environmental challenges [7].Vegetable oil can be used to prepare biohydrocarbon fuel through transesterification, esterification, pyrolysis, gasification, and catalytic cracking reactions [8]. The current process for preparing biofuels from vegetable oils is transesterification to produce biodiesel (fatty acid methyl ester), but it has been found that the biodiesel has the disadvantages of low calorific value, high kinematic viscosity, and low temperature stability [9, 10].

Corn oil and soybean oil are used to produce biodiesel, but they occupy the resources of edible oil [11, 12]. Therefore, the development of new resources to produce biodiesel has attracted the attention of many researchers, such as *Mangiti* oil, *baobab* oil, *date palm* oil, *Jatropha* seed oil, *Manchurian apricot* oil, and *Siberian apricot* Oil [13–20]. In a study, *Xanthium strumarium* plant stems have been pyrolyzed with catalysts (ulexite, colemanite, and borax) and without catalysts at temperatures of 350–550°C. The catalyst and temperature were found to be effective on the conversion. The highest liquid product yield is obtained with colemanite catalyst at 550°C as 27.97%. It has been identified that the liquid product comprised aliphatic, aromatic, and heterocyclic compounds [21]. Another study found that the liquid and solid products obtained by pyrolysis of *Lactuca scariola* under different catalysts and temperatures are products with higher energy value and can also be used as alternative energy sources [22]. As a result of the study, black cumin seed cake (BCSC) was converted into liquid and solid products with the pyrolysis method. The highest conversion

rate was obtained in the presence of Al_2O_3 (78.91%) and $SnCl_4{\cdot}5H_2O$ (76.06%) catalysts at 500°C [23]. In these vegetable oils, *Swida wilsoniana* oil is a very useful oil which has high oil content [24, 25]. There are 77.68% the fatty acid oleic acid and linoleic acid in *Swida wilsonian* oil [26], so it can be used as a raw material for the production of biodiesel.

Swida wilsoniana oil is mainly prepared by thermal cracking, catalytic cracking, and transesterification [27, 28]. *Swida wilsoniana* oil from direct thermal cracking and catalytic cracking has low temperature fluidity and low calorific value, which limits its wide application [29–32]. At present, it has received widespread attention that the first-generation biodiesel converts to hydrocarbon-rich liquid fuel by catalytic hydrogenation. Ouyang et al. [33] used fatty acid methyl ester hydride-oxygenation to prepare second-generation biodiesel with a conversion rate of 99.52 %. Zuo Hualiang et al. [34] found that Ni-supported catalysts have higher hydride-oxygenation performance, while maintaining higher alkane selectivity. Dhanalaxmi et al. have successfully designed a porous organic polymer-encapsulated (PPTPA-1) nanohybrid magnetically retrievable Pd-Fe_3O_4 catalyst in a one-step solvothermal route with a Pd: Fe (1 : 9) ratio which exhibited an outstanding higher activity over their monometallic counterparts for selective LA hydrogenation to GVL, a key platform molecule in many biorefinery schemes [35]. An experimental data suggested that a novel porous organic network material (TpPON) can be synthesized via a one-step acid-catalyzed condensation reaction between 1, 3, 5-triformylphloroglucinol and triphenylamine. Ru NPs have been successfully deposited at the surfaces of TpPON to obtain the Ru nanoparticles-decorated Ru@TpPON, which showed excellent catalytic activity in the hydrodeoxygenation of various oils to furnish long-chain alkanes (biodiesel) [36]. Wang et al. [37] used soybean oil as the raw material supported Ni and Mo metals on the ZSM-5 carrier to prepare liquid fuel. Wang Fei et al. [38] found that when a molecular sieve is used as a carrier in the hydrogenation of oils and fats, a higher yield of isomerized hydrocarbon products could be obtained. The key to get a higher yield is to choose the right oil hydrogenation catalyst [39]. Ni as an inexpensive transition metal has received widespread attention due to the high hydrogenation activity [40, 41].

Therefore, the purpose of this research is to study the interaction between independent variables (catalyst addition level, reaction temperature, and reaction pressure) and dependent variables by the response surface methodology and optimize the preparation conditions. On the other hand, we found that biohydrocarbon fuels produced by hydrogenation will be closer to the existing fossil fuels.

2. Materials, Instruments, and Methods

2.1. Materials and Instruments. *Swida wilsoniana* pyrolysis products were prepared from the laboratory of the Hunan Academy of Forestry Science. The ZSM-5 zeolite molecular sieve (Si : Al = 23 : 1) was from Alfa Essa Chemical Co., Ltd., China. Hydrogen (purity: 99.99%) was purchased from Huazhong Special Gas Co., Ltd., Hunan. Ni $(NO_3)_2{\cdot}6H_2O$ and other chemicals were of analytical grade and purchased from Sinopharm Chemical Reagent Co., Ltd., China.

A controller (Parr 4848, Parr Instrument Co., Ltd.); high-pressure reactor (Parr 4568, Parr Instrument Co., Ltd.); Fourier infrared spectrometer (IS5, Thermo Fisher, USA); electronic analytical balance (AUY-220, Shimadzu Co., Ltd.); single four-stage bar GC-MS (Scion-SQ, Bruker Co., Ltd.); and element analyzer (Vario EL-III, Elementar Co., Germany) were used.

2.2. Preparation of the Ni-ZSM-5 Catalyst. The Ni-ZSM-5 catalyst loaded with nickel metal was prepared by the equal volume impregnation method: First, 15 g ZSM-5 was weighed into a quartz crucible and activated in a muffle furnace at 400°C for a certain period of time. Then, the nickel nitrate hexahydrate solution was mixed and stirred at a constant temperature overnight. After being left to stand for 10.0 h, it was dehydrated and dried. It continued to be roasted at a certain temperature to a set time and, finally, waited for cooling, milling, sieving, and reduction.

2.3. Method for Preparing Swida wilsoniana Pyrolysis Products. *Swida wilsoniana* oil was used as the raw material for the catalytic pyrolysis reaction. The specific operation steps are as follows: 250 g of *Swida wilsoniana* oil and 1.0 wt.% La_2O_3 are introduced into a straight three-port glass reactor, mixed evenly, and sealed with a stopper and heated to 500°C, and the collected liquid fuel is condensed by using the condenser after 80 minutes, which is the product of the pyrolysis of *Swida wilsoniana*.

2.4. Hydrogenation Effect of Pyrolysis Products. The hydrogenation effect of the pyrolysis product of the *Swida Wilsoniana* was used to evaluate the conversion rate of unsaturated components by the change of the iodine value before and after the reaction. The iodine value was determined according to the Chinese National Standard GB5532-2008.

$$Y\% = \frac{C_a - C_0}{C_0} \times 100\%, \tag{1}$$

where C_a is the iodine value of the product after the reaction, g/100 g; C_0 is the initial iodine value of the *Swida wilsoniana* pyrolysis products, g/100 g.

2.5. Method for Catalytic Hydrogenation of Pyrolysis Products

2.5.1. Single-Factor Design for Conversion Rates. The factors influencing the hydrogenation of pyrolysis products are the addition of a catalyst, reaction temperature, reaction pressure, and reaction time. First, we add 100 g of the pyrolysis product and the Ni-ZSM-5 catalyst (0.4 wt.%, 0.6 wt.%, 0.8 wt.%, 1.0 wt.%, 1.2 wt.%) in a high-pressure reactor. Second, it is connected to nitrogen gas for 8 to 10 min. Third, the vent valve is closed, and the parameters of the high-pressure reactor are adjusted from the operating end: reaction pressure (1.0 MPa, 1.5 MPa, 2.0 MPa, 2.5 MPa, and 3.0 MPa), reaction temperature (110°C, 140°C, 170°C, 200°C, and

230°C), after the reactor reaches the corresponding conditions, and start timing (60 min, 90 min, 120 min, 150 min, and 180 min) of the catalytic hydrogenation reaction to the end of the reaction. Finally, the condensed gas collected by using the collector is the biofuel; Figure 1 represents the catalytic hydrogenation process flow.

2.5.2. Response Surface Methodology (RSM) Experimental Design. Software Design-Expert (Trial Version 10.0.1.0, Stat-Ease Inc., Minneapolis, USA) was employed for experimental design. Based on the single-factor test, the catalytic addition level, reaction temperature, and reaction pressure were selected as independent variables, and the conversion rate of unsaturated components was the dependent variable. The independent variables and their levels are presented in Table 1. Similarly, the results of the whole design comprising 17 experimental points performed in randomized order are presented in Table 2.

2.6. Product Characterization Methods

2.6.1. Elemental Analysis. A constant element analyzer was used to detect the content of carbon, nitrogen, and hydrogen in pyrolysis products and biohydrocarbon fuels, and, then, the oxygen content was obtained by subtraction.

2.6.2. Infrared Spectroscopy. The detector is a midinfrared DTGS detector with a wavenumber scanning range of 400–4000 cm^{-1} and a resolution of 4.0 cm^{-1}.

2.6.3. GC-MS Analysis. The components of hydrocarbon biofuels analysis were performed by GC-MS with a Scion-SQ single quadrupole mass spectrometer and electron bombardment (EI) ion source; the electron energy is 70 eV, the quadrupole temperature is 150°C, the ion source temperature is 230°C, and the mass scanning range is 33 ~ 350 u.

2.6.4. Performance Analysis. The product was analyzed according to the Chinese National Standard GB19147-2016 (vehicle diesel).

3. Results and Discussion

3.1. Catalytic Characterization Analysis

3.1.1. N_2 Adsorption-Desorption Isotherms Analysis. Figure 2 shows the N_2 adsorption-desorption isotherms of the ZSM-5 and Ni-ZSM-5. The pore structure parameters of ZSM-5 and Ni-ZSM-5 are shown in Table 3.

It can be seen from Figure 2(b) that the isotherm of ZSM-5 is of type IV, which changes strongly at a relative pressure of 0.4 to 0.8 and has an obvious H4 hysteresis loop. The appearance of the hysteresis ring indicates that ZSM-5 is a mesoporous molecular sieve. It can be seen from Figure 2(a) that the isotherm of Ni-ZSM-5 is also of type IV, indicating that the catalyst maintains the structural characteristics of the carrier ZSM-5 after supporting the nickel metal active material and has a stable crystal frame support.

It can be seen from Table 3 that ZSM-5 has a high specific surface area (268.825 m^2/g) and an average pore diameter of 2.276 nm. However, compared with the ZSM-5 carrier, the Ni-ZSM-5 specific surface area and pore volume decrease, but the change is not obvious. This is because of the accumulation effect on the ZSM-5 carrier after loading nickel. The reason why the average pore diameter becomes larger is that the nickel metal enters the carrier ZSM-5's skeleton to replace Si or Al, and it is verified that the nickel metal is supported on the carrier ZSM-5.

3.1.2. XRD Analysis. XRD characterization of ZSM-5 and Ni-ZSM-5 is shown in Figure 3. As can be seen from Figure 3, the characteristic peak of the Ni-ZSM-5 catalyst (a) appeared at $2\theta = 8°$, 9°, 23°, 24°, and 45°, but the strength changed, indicating that the basic skeleton structure of the Ni-ZSM-5 catalyst was not damaged after loading the nickel active substance. The XRD pattern of the Ni-ZSM-5 catalyst (a) showed an obvious characteristic peak of Ni at $2\theta = 44.5°$, 51.8°, and 76.4°, indicating that the active component Ni in the Ni-ZSM-5 catalyst had small particle size and high dispersion state, and the catalyst Ni-ZSM-5 had high catalytic activity.

3.1.3. SEM Analysis. The results of SEM characterization of ZSM-5 and Ni-ZSM-5 (21wt. %Ni), respectively, are shown in Figure 4. According to A1 and A2 in Figure 4, it can be seen that the ZSM-5 carrier is a flake smooth crystal and the overall appearance is irregular and round, which is the characteristic morphology of a typical ZSM-5 molecular sieve. Compared with ZSM-5, the Ni-ZSM-5 catalyst supported with nickel metal active substances of B1 and B2 attached spherical particles with a diameter of less than 100 nm on the grain surface, which confirmed that Ni-ZSM-5 presented nickel agglomeration, multiple active points, and good loose dispersion.

3.1.4. FT-IR Analysis. FT-IR characterization of ZSM-5 and Ni-ZSM-5 catalysts was carried out, respectively, and the results are shown in Figure 5. ZSM-5 in 1085.85 cm^{-1} infrared transmission peaks can be ascribed to the skeleton structure of SiO_4 or AlO_4 tetrahedron internal antisymmetric vibration, 790.79 cm^{-1} transmission peak belongs to skeleton SiO_4 or internal symmetry vibration AlO_4 tetrahedron, 1219.15 cm^{-1} transmission peak corresponds to the SiO_4 or stretching vibration of AlO_4 tetrahedron, and 452.92 cm^{-1} transmission peak corresponds to the skeleton SiO_4 or bending vibration of AlO_4 tetrahedron. By comparing *a* and *b* spectra, it can be seen that similar infrared characteristic peaks appear at the same position on Ni-ZSM-5, and the intensity of the peaks changes, indicating that Ni-ZSM-5 maintains the original skeleton structure and Ni successfully enters into the molecular sieve skeleton.

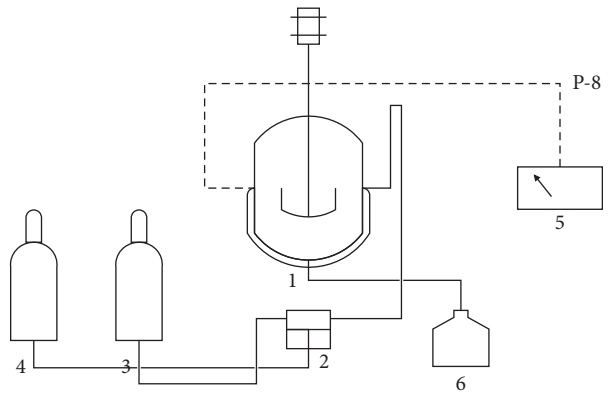

Figure 1: Process diagram of the catalytic hydrogenation unit. 1. High-pressure reactor; 2. no power booster; 3. hydrogen source; 4. nitrogen source; 5. controller; and 6. liquid collector.

Table 1: Box–Behnken experimental factor level.

Factors	Run number	Level		
		−1	0	1
Ni-ZSM-5 addition level (wt.%)	A	0.8	1.0	1.2
Reaction temperature (°C)	B	140	170	200
Reaction pressure (MPa)	C	1.5	2.0	2.5

Table 2: Response surface experiment design and results.

Run number	Ni-ZSM-5 addition level (A, %)	Reaction temperature (B, °C)	Reaction pressure (C, MPa)	Conversion rate (Y, %)
1	0	−1	1	89.01
2	0	1	1	92.46
3	1	0	−1	91.19
4	0	0	0	98.48
5	1	1	0	92.25
6	0	0	0	96.86
7	−1	1	0	88.50
8	0	−1	−1	89.69
9	−1	−1	0	86.35
10	0	1	−1	88.15
11	0	0	0	97.84
12	−1	0	1	87.69
13	1	−1	0	90.70
14	−1	0	−1	84.31
15	1	0	1	90.19
16	0	0	0	97.34
17	0	0	0	98.58

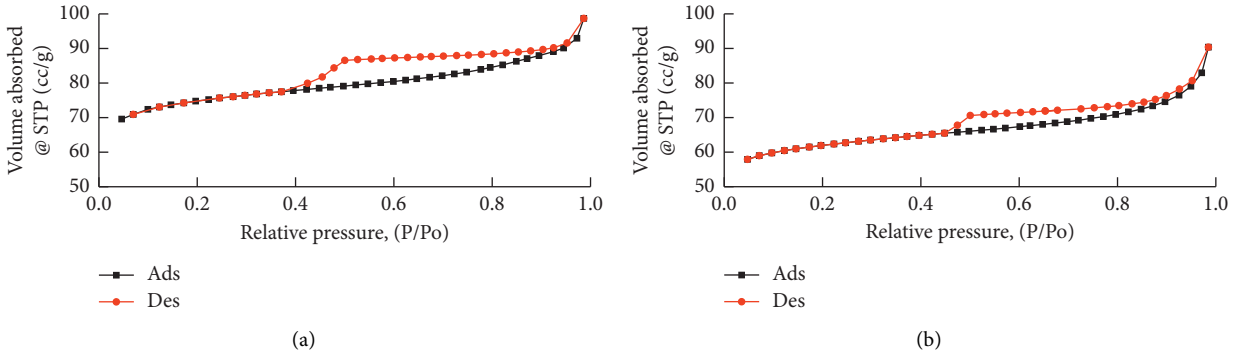

Figure 2: N_2 adsorption-desorption isotherms of the ZSM-5 and Ni/ZSM-5 catalysts. (a) Ni-ZSM-5; (b) ZSM-5.

Table 3: Pore structure parameters of ZSM-5 and Ni-ZSM-5 catalysts.

Sample	Specific surface area S/(m^2•g^{-1})	Pore volume V/(ml•g^{-1})	Pore diameter D/(nm)
ZSM-5	268.835	1.531	2.276
Ni-ZSM-5	221.771	1.400	2.527

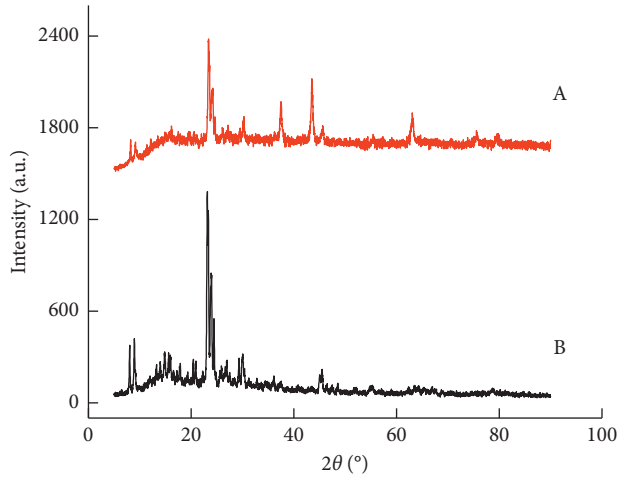

Figure 3: XRD patterns of the ZSM-5 and Ni-ZSM-5 catalysts. A. Ni-ZSM-5; B. ZSM-5.

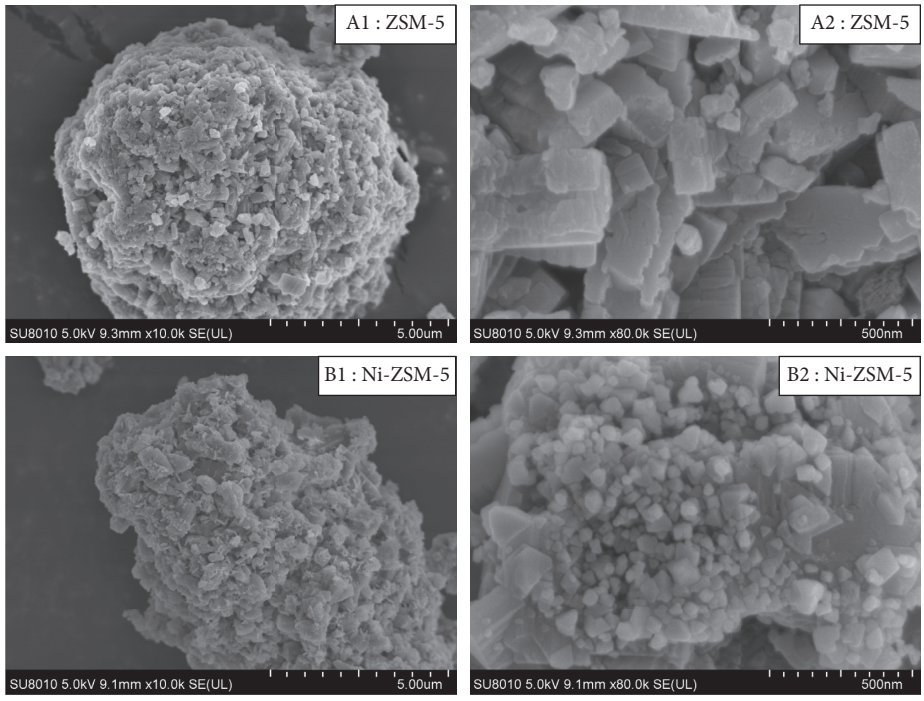

Figure 4: SEM image of ZSM-5 and Ni/ZSM-5 catalysts.

3.1.5. NH3-TPD Analysis. The results of NH3-TPD characterization of ZSM-5 and Ni-ZSM-5, respectively, are shown in Figure 6.

As shown in Figure 6, ZSM-5 has two wide peaks at 150 ~ 550°C. Among them, the low-temperature peak (180°C) is generated during the desorption of NH_3 due to weak adsorption. The high-temperature peak (480°C) is generated by NH_3 desorption adsorbed on the strong acid position of the molecular sieve. The area of the NH_3 desorption peak can be used to measure the amount of acid in the catalyst. The Ni in Ni-ZSM-5 treated with nickel-loaded active material interacts with the acid site on ZSM-5 to form strongly acidic $[Ni(OH)]^+$ groups and form stronger acid sites, thus increasing the area of the high-temperature

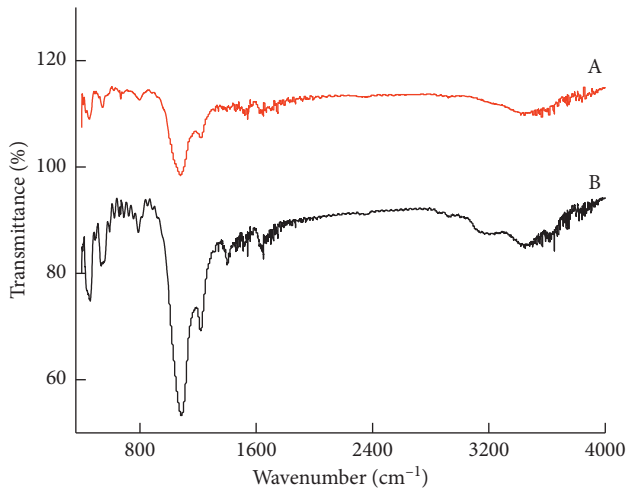

Figure 5: FT-IR spectra of ZSM-5 and Ni-ZSM-5 catalysts. A. Ni-ZSM-5; B. ZSM-5.

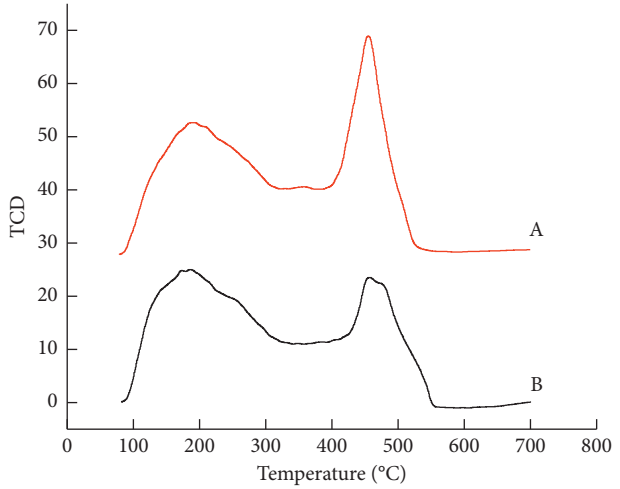

Figure 6: NH3-TPD profiles of ZSM-5 and Ni-ZSM-5 catalysts. A. Ni-ZSM-5; B. ZSM-5.

desorption peak. The acid content of ZSM-5 and Ni-ZSM-5 was quantitatively analyzed, and the results are shown in Table 4. It can be seen from the table that the acid content (4.8370 mmol·g^{-1}) of the catalyst loaded with nickel active substances was significantly greater than that of ZSM-5 (3.4085 mmol·g^{-1}).

3.2. Single-Factor Experimental Analysis

3.2.1. Effect of the Ni-ZSM-5 Addition Level on the Conversion Rate of Unsaturated Components. The effect of the Ni-ZSM-5 addition level on the conversion rate of unsaturated components is shown in Figure 7. The Ni-ZSM-5 addition level refers to the mass fraction relative to the pyrolysis product. The conversion rate was determined by applying the Ni-ZSM-5 addition level ranging from 0.4 wt.% to 1.2 wt.% with the other reaction conditions as follows: the reaction temperature was 200°C, the time was 180 min, and the pressure was 2.0 MPa. When the catalyst addition level was 1.0 wt.%, the conversion rate reached the peak, and then, when the addition level of Ni-ZSM-5 was increased, there was no obvious effect on the conversion rate. Because the addition level of the catalyst used in the early stage was small, so was the number of active sites, and the catalytic reaction cannot be fully completed within the investigation period. The conversion rate will increase with the addition level of the catalyst. Considering the cost and conversion effect, the optimal condition in the present experiment should be ranged from 0.8 wt. % to 1.2 wt.%.

Table 4: Acidity of ZSM-5 and Ni-ZSM-5 catalysts.

Sample	Acidity (mmol·g^{-1})
ZSM-5	3.4085
Ni-ZSM-5	4.8370

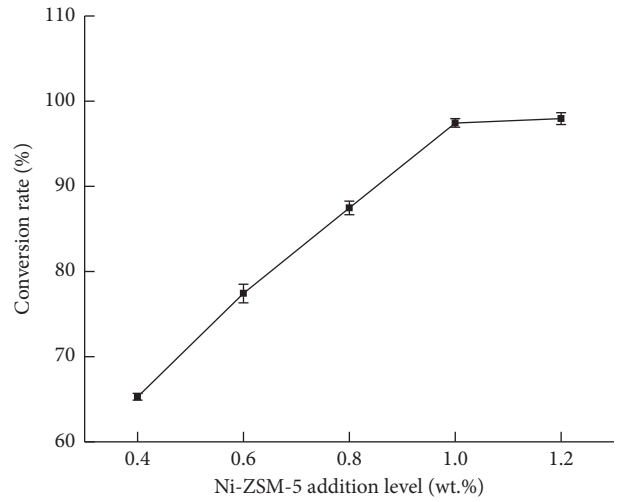

Figure 7: Effects of the Ni-ZSM-5 addition level on the conversion rate of unsaturated components.

3.2.2. Effect of Reaction Temperature on the Conversion Rate of Unsaturated Components. Figure 8 shows that the reaction temperature is an important factor affecting the hydrogenation reaction. With the increase of temperature (120 ~ 170°C), the hydrogenation conversion rate of the pyrolysis products of *Swida wilsoniana* oil significantly increased, and their value reached the maximum when the reaction temperature was 170°C. This is because catalytic hydrogenation is an exothermic reaction, and the preheating is to provide the initial starting energy of the reaction for the hydrogenation catalyst. Once the reaction starts, other means need to be used to release part of the thermal energy.

3.2.3. Effect of Reaction Pressure on the Conversion Rate of Unsaturated Components. By fixing the Ni-ZSM-5 addition level of 1.0 wt.%, reaction temperature of 170°C, and reaction time of 180 min, respectively, the effects of reaction pressure ranging from 1.0 to 3.0 MPa were studied. Figure 9 shows that as the reaction pressure increased, the conversion rate of

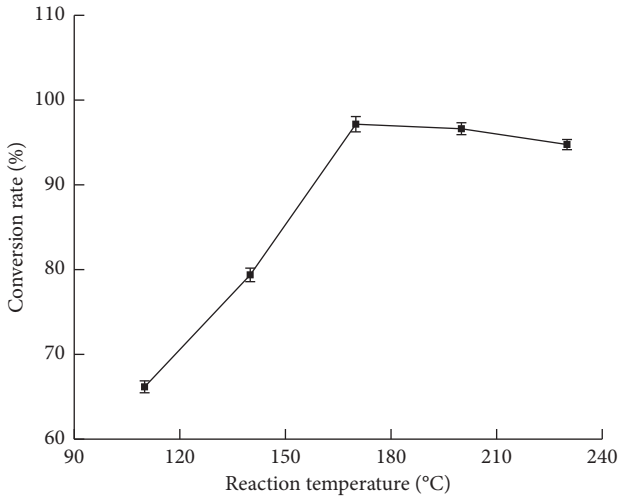

Figure 8: Effects of reaction temperature on the conversion rate of unsaturated components.

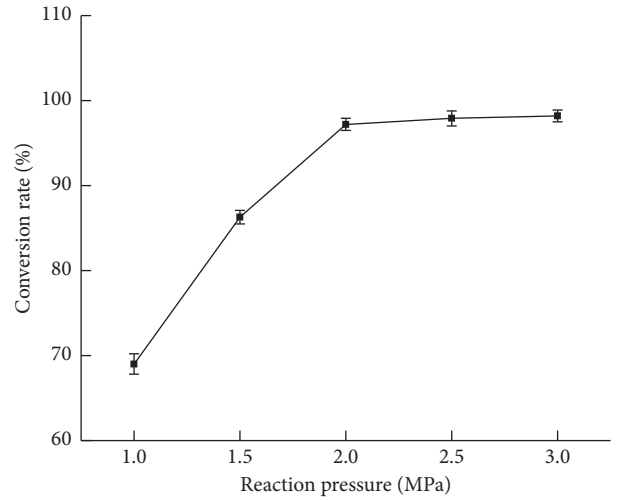

Figure 9: Effects of reaction pressure on the conversion rate of unsaturated components.

unsaturated components increased significantly, and after 2.0 MPa, it showed a small increase. The reason was that the higher the pressure, the greater the solubility of the pyrolysis products of *Swida wilsoniana*. The contact area of hydrogen with the catalyst became larger, which in turn, accelerated the reaction rate and promoted the chemical equilibrium to proceed in the positive direction. However, too high pressure could also increase the equipment cost, so the reaction pressure was chosen to be 2.0 MPa.

3.2.4. Effect of Reaction Time on the Conversion Rate of Unsaturated Components. Under the conditions of the Ni-ZSM-5 addition level of 1.0 wt.%, reaction temperature of 170°C, and reaction pressure of 2.0 MPa, the influence of the reaction time in the range of 60 min to 180 min was studied. Figure 10 shows that as the reaction time increased, the conversion of unsaturated components in the

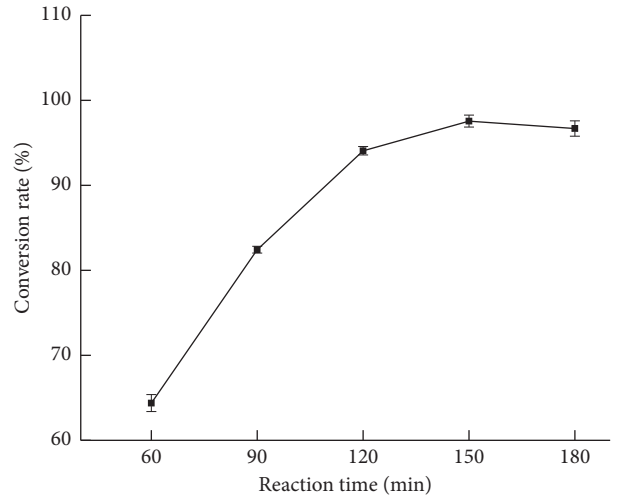

Figure 10: Effects of reaction time on the conversion rate of unsaturated components.

pyrolysis products increased significantly. However, when the reaction time was 150 min, the reaction reached the equilibrium point, and then, when the reaction time was increased, the conversion rate was basically unchanged. Considering and simplifying the follow-up experiment comprehensively, the reaction time was chosen to be 150 min.

3.3. Statistical Analysis and Model Fitting. As shown in Table 5, through the analysis of the experimental results by Design-Expert software, the quadratic regression equation between the Ni-ZSM-5 addition level (A/%), reaction temperature (B/°C), and reaction pressure (C/MPa) factors and the conversion rate of unsaturated components in the process of the hydrogenation reaction of *Swida wilsoniana* pyrolysis products could be expressed by the following second-order polynomial equation:

$$Y = 97.82 + 2.19 \times A + 0.70 \times B + 0.75 \times C - 0.15 \times A \times B - 1.10 \times A \times B + 1.25 \times B \times C - 4.93 \times A^2 - 3.44 \times B^2 - 4.55 \times C^2. \quad (2)$$

The quality of the fit of the polynomial model equation was assessed by the coefficient of determination (R) and ANOVA. The significance of the regression coefficient was evaluated by checking the F value and p value.

The absolute value of the corresponding coefficient of the factor in the model equation was the degree of influence of the factor on the reaction conversion rate, and the positive and negative coefficients reflect the direction of influence. According to the size of the coefficient, it can be seen that the Ni-ZSM-5 addition level (A)> reaction pressure (C)> reaction temperature (B), the Ni-ZSM-5 addition level had the most significant effect on the conversion rate, and there was an interaction between the three factors.

Table 5: Variables and levels used in RSM design.

Source	SS	Df	MS	F value	p value	Significance*
Model	324.30	9	36.03	85.03	<0.0001	***
A	38.19	1	38.19	90.13	<0.0001	***
B	3.93	1	3.93	9.28	0.0187	*
C	4.52	1	4.52	10.65	0.0138	*
AB	0.090	1	0.090	0.21	0.6589	
AC	4.80	1	4.80	11.32	0.0120	*
BC	6.23	1	6.23	14.69	0.0064	**
A^2	102.18	1	102.18	241.14	<0.0001	***
B^2	49.93	1	49.93	117.84	<0.0001	***
C^2	87.12	1	87.12	205.60	<0.0001	***
Residual	2.97	7	0.42			
Lake of fit	0.80	3	0.27	0.49	0.7062	
Pure error	2.17	4	0.54			
Correlation total	327.26	16				

R-squared = 0.9909; adj R-squared = 0.9793; pred R-squared = 0.9505

Note: ***is a very significant level ($p \le 0.0001$), **is a highly significant level ($0.001 \le p \le 0.01$), *is a significant level ($0.01 \le p \le 0.05$).

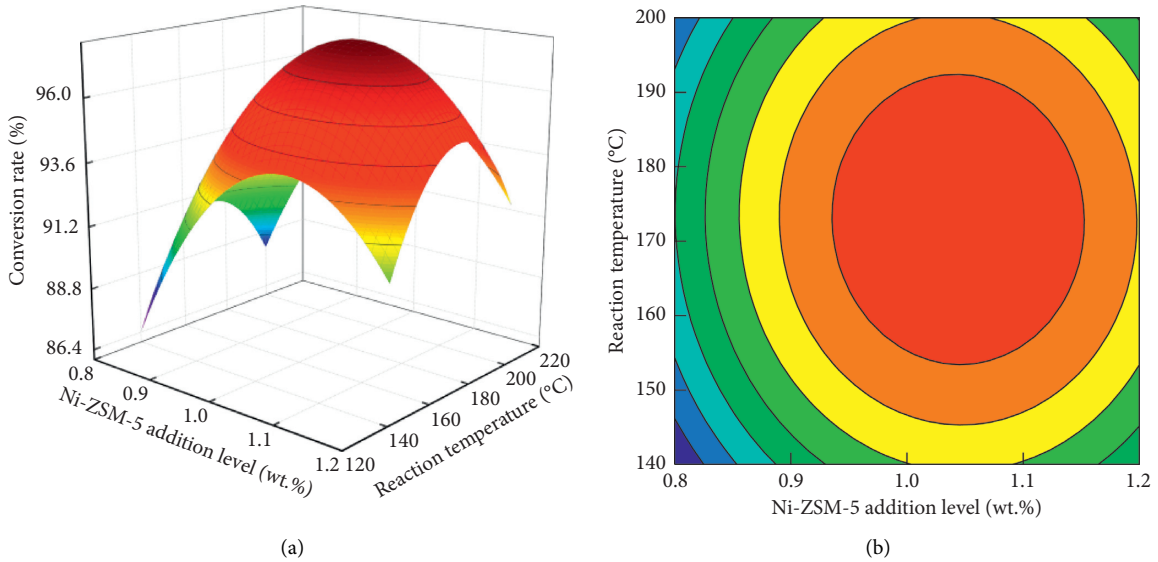

Figure 11: The effect of the Ni-ZSN-5 addition level and reaction temperature on conversion.

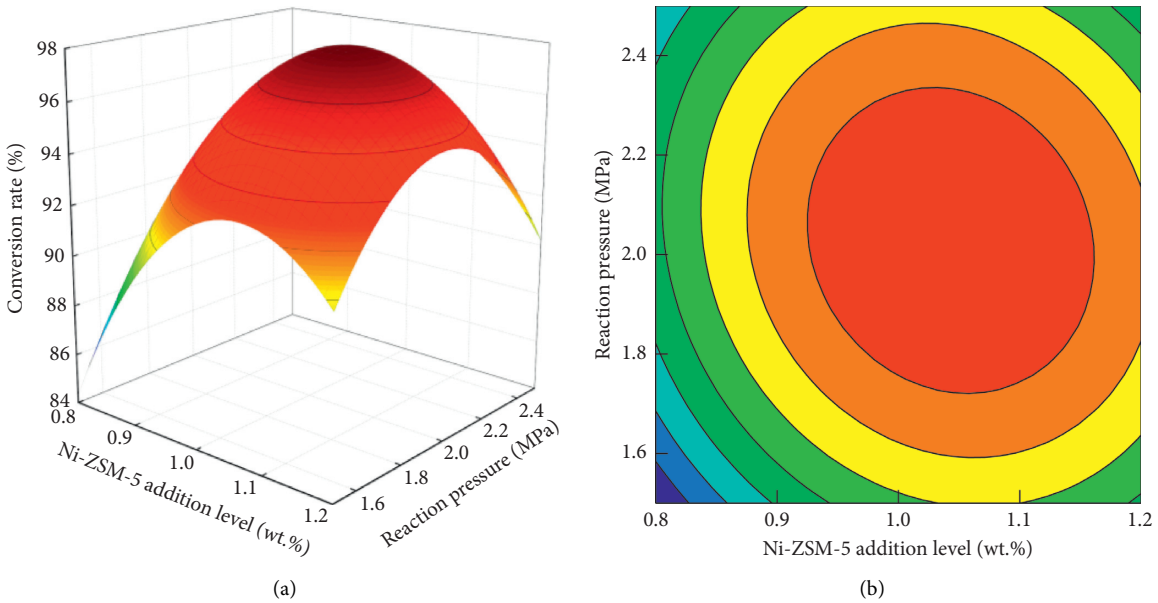

Figure 12: The interaction of the Ni-ZSN-5 addition level and reaction pressure on conversion.

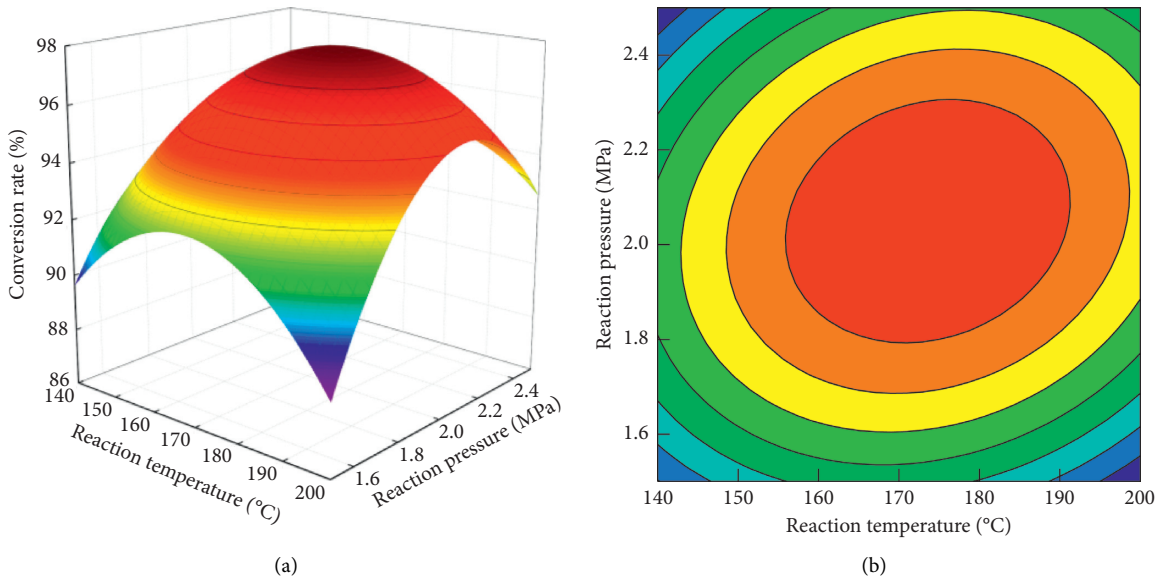

Figure 13: Effect of reaction temperature and pressure on conversion.

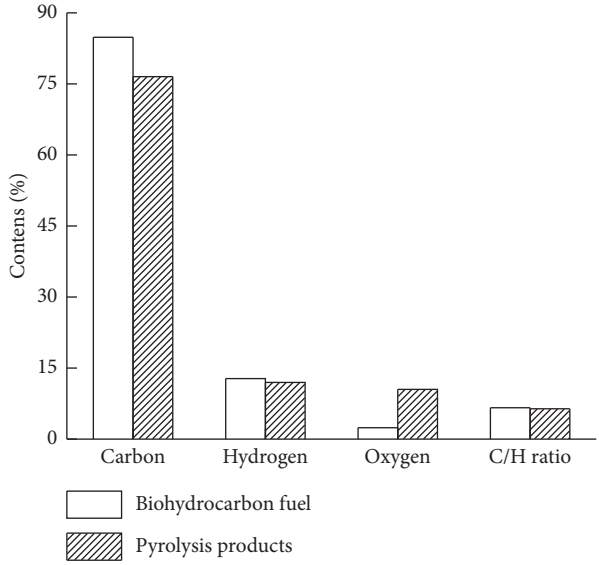

Figure 14: Element analysis of pyrolysis products and biohydrocarbon fuel.

3.4. Analysis of the Response Surface. According to the abovementioned regression equation, through software analysis, the surface curve and contour map of the effect of multiple conversions of the interaction surface curve factors (Ni-ZSM-5 addition level (A)> reaction pressure (C)> reaction temperature (B)) were obtained.

As shown in Figures 11–13, the three interactions were all convex spherical surfaces, indicating that there was the highest point of the response value (conversion rate) within the range of conditions under investigation. The Ni-ZSN-5 addition level had the most significant effect on the conversion rate, which was characterized by a steep surface, followed by reaction pressure and temperature.

3.5. Optimization of Modification Conditions and Model Validation. The optimal conditions obtained from the response surface are the Ni-ZSM-5 addition level 1.04 wt.%, reaction temperature 173.30°C, and reaction pressure 2.04 MPa, and the optimal simulated value of the unsaturated component conversion rate under this condition is 98.12%. In order to facilitate the actual operation, the best process is modified to 1.05 wt.% Ni-ZSM-5 addition level, 173°C reaction temperature, and 2.00 MPa reaction pressure.

Repeated experiments verified the reliability of the results, and the conversion rate of unsaturated components was 98.10%, which was close to the simulated value. This indicated that it is reliable to use the response surface

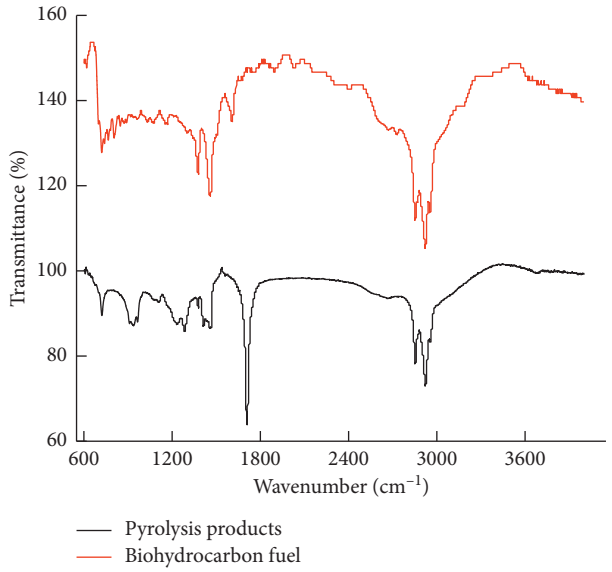

Figure 15: FT-IR spectra of pyrolysis products and biohydrocarbon fuel.

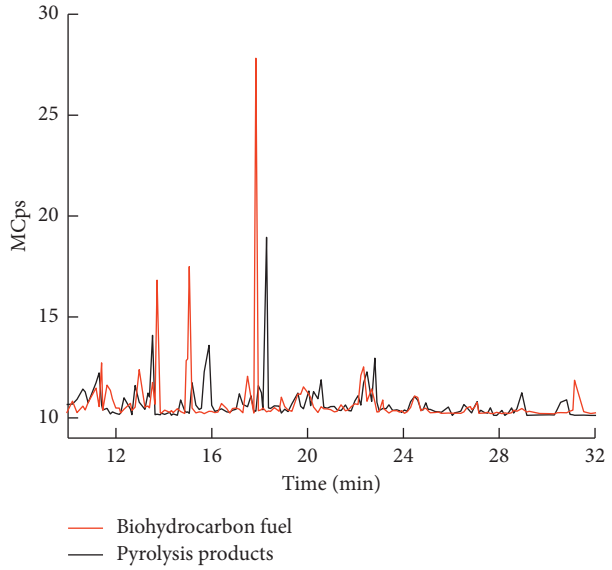

Figure 16: GC-MS spectra of pyrolysis products and biohydrocarbon fuel.

method to optimize the process conditions of the hydrogenation reaction of *Swida wilsoniana* pyrolysis products.

3.6. Reaction Product Analysis Results

3.6.1. Elemental Analysis. Figure 14 shows that, after the catalytic hydrogenation of the light-skinned pyrene-based pyrolysis products, the contents of C and O elements have changed significantly, and the C element content increased from 76.53% to 84.83%, but the O element content decreased from 11.50% to 2.39%, The C/H ratio is 6.639.

It can be seen from this that this study effectively promoted the hydrogenation and deoxygenation pathways of the pyrolysis product of the light-bark-based wood.

3.6.2. FI-IR Analysis. As shown in Figure 15, the infrared spectra difference of the pyrolysis products and biohydrocarbon fuel is mainly reflected in the 915 ~ 955 cm^{-1}, 1700 ~ 1750 cm^{-1}, and 2600 ~ 3800 cm^{-1}wave bands.

The-OH contraction vibration peak of the biohydrocarbon fuel disappeared at 915 ~ 955 cm^{-1}, and the C = O contraction vibration peak disappeared at 1700 ~ 1750 cm^{-1}, but the intensity of the saturated C-H stretching vibration peak increased at 2600–2800 cm^{-1}, indicating that, after hydrogenation, the alkane content increased and some oxygen was removed.

3.6.3. GC-MS Analysis. GC-MS characterization was performed on *Swida wilsoniana* pyrolysis products and

Table 6: Composition and carbon chain distribution of pyrolysis products and biohydrocarbon fuels.

Sample	Carbon chain distribution			Composition			
	$C_3 \sim C_7$ (%)	$C_8 \sim C_{19}$ (%)	$>C_{19}$ (%)	Alkane (%)	Olefin (%)	Aromatic (%)	Oxygenate (%)
Pyrolysis products	23.95	44.16	31.89	34.71	25.13	24.03	21.13
Biohydrocarbon fuel	27.89	62.75	9.36	42.86	30.08	21.42	5.64

Table 7: Analysis of fuel performance.

Performance	*Swida wilsoniana* pyrolysis products	Biohydrocarbon fuel	0# diesel oil (GB-19147 2016)
Density (20°C g/mL)	0.89	0.87	0.865
Kinematic viscosity ($mm^2 \cdot s^{-1}$)	4.46	3.54	3.0–8.0
Sulfur content% (m/m)	0.022	0.013	< 0.3
Flash point°C	54	66	> 55
Mechanical impurities% (m/m)	0	0	0
Acid value (mg KOH/g)	120.42	0.12	0.09
Copper corrosion	1a	1a	1a
Freezing point°C	0	−12	0
Calorific value (MJ/kg)	36.42	42.72	43.559

biohydrocarbon fuels. It can be seen from Figure 16 and Table 6 that the total amount of biohydrocarbon compounds increased significantly, up to 94.36%. The content of unsaturated components was reduced. At the same time, the content of carbon chain C_3–C_7 in the biohydrocarbon fuel increased by 3.95%, C_8–C_{19} increased from 44.16% to 62.75%, and the carbon chain content after C_{19} decreased to 9.37%.

3.6.4. Performance Analysis. A series of fuel performance analysis were carried out on the products of *Swida wilsoniana* pyrolysis products after Ni- ZSM-5 catalytic hydrogenation. The results are shown in Table 7. The performance indicators of petrochemical diesel include the cetane number, density, oxidation stability, kinematic viscosity, acid value, condensation point, and calorific value. Through comparison, it was found that the biohydrocarbon fuel prepared by the hydrogenation reaction of the *Swida wilsoniana* pyrolysis products had a higher calorific value.

4. Conclusions

In this study, on the basis of the single-factor experiment, the response surface method was used to further optimize the hydrogenation process and the influence of the addition of catalyst, reaction temperature, reaction time, and reaction pressure on the conversion of *Swida wilsoniana* hydrocarbons. Different analysis methods (GC-MS, elemental, FT-IR, performance) were used to analyze the obtained liquid. According to the results, the highest conversion rate was 98.10% when the catalyst dosage was 1.05 wt.%, the reaction temperature was 173°C, and the reaction pressure was 2.00 MPa. The results of GC-MS, elements, and FT-IR used to characterize the products support each other. The results of the research show that *Swida wilsoniana*-decomposed products can be transformed into high-quality biofuels by the catalytic hydrogenation of Ni-ZSM-5 and can be used as an alternative energy source.

Data Availability

The data used to support the findings of this study are available from the corresponding author upon request.

Conflicts of Interest

The authors declare that they have no conflicts of interest.

Acknowledgments

This work was supported by the grant from National Key R&D Program of China (2019YFB1504001) and Forestry Science and Technology Demonstration Project Funds of Central Finance (2019[XT]004).

References

[1] C. K. Zhang, W. D. Niu, S. M. Zhao, Y. Z. Zhang, and Z. F. Niu, "Research and thoughts on global energy shortage," *Journal of State Grid Technology College*, vol. 22, no. 2, pp. 36–38, 2019.

[2] Y. Yang and C. X. Tian, "Current status and development strategies of biodiesel industry in China," *Journal of the Chinese Cereals and Oils Association*, vol. 25, no. 2, pp. 150–154, 2010.

[3] R. K. Liu, X. P. Yang, R. X. Wang, and Y. J. Zhang, "Advances in catalyst used in oil transesterification for preparing diesel," *Journal of the Chinese Cereals and Oils Association*, vol. 21, no. 3, pp. 273–276, 2006.

[4] J. Ma, X. Y. Ma, and Q. Liu, "Utilization and research progress of biomass energy," *Journal of Anhui Agricultural Sciences*, vol. 40, no. 4, pp. 2202–2206, 2012.

[5] C. Z. Wu, Z. Q. Zhou, X. L. Yin, and W. M. Yi, "Current status of biomass energy development in China," *Transactions of the Chinese Society for Agricultural Machinery*, vol. 40, no. 1, pp. 91–99, 2009.

[6] L. L. Ma, "Process technology of bio-energy utilization and its development," *Chemical Industry*, vol. 25, no. 8, pp. 9–14, 2007.

[7] C. Li, D. Liu, S. Ramaswamy, and J. Yan, "Biomass energy and products: advanced technologies and applications," *Applied Energy*, vol. 157, no. 1, pp. 489-490, 2015.

[8] M. Jahirul, M. Rasul, A. Chowdhury, and N. Ashwath, "Biofuels production through biomass pyrolysis-a technological review," *Energies*, vol. 5, no. 12, pp. 4952–5001, 2012.

[9] S. Wang, Y. L Zhai, F. S. Li, H. L. Luo, and Y. Chen, "Liquid fuel characteristics of 16 kinds of biodiesels," *China Oils and Fats*, vol. 44, no. 12, pp. 45–50, 2019.

[10] G. Wu, G. H. Jiang, and Z. Y. Yang, "Particulate matter generation and emission characteristics of diesel engine fueled by biodiesel," *Research of Environmental Sciences*, vol. 32, no. 11, pp. 1809–1817, 2019.

[11] M. Atapour and H.-R. Kariminia, "Characterization and transesterification of iranian bitter almond oil for biodiesel production," *Applied Energy*, vol. 88, no. 7, pp. 2377–2381, 2011.

[12] C. E. Goering, A. W. Schwab, M. J. Daugherty, E. H. Pryde, and A. J. Heakin, "Fuel properties of eleven vegetable oils," *Transactions of the ASAE*, vol. 25, no. 6, pp. 1472–1477, 1982.

[13] M. A. Amani, M. S. Davoudi, K. Tahvildari, S. M. Nabavi, and M. S. Davoudi, "Biodiesel production from phoenix dactylifera as a new feedstock," *Industrial Crops and Products*, vol. 43, pp. 40–43, 2013.

[14] A. Demirbas, "Utilization of date biomass waste and date seed as bio-fuels source," *Energy Sources, Part A: Recovery, Utilization, and Environmental Effects*, vol. 39, no. 8, pp. 754–760, 2017.

[15] M. Farooq, A. Ramli, A. Naeem et al., "Biodiesel production from date seed oil (Phoenix dactylifera L.) via egg shell derived heterogeneous catalyst," *Chemical Engineering Research and Design*, vol. 132, pp. 644–651, 2018.

[16] J. C. Gomes Filho, A. S. Peiter, W. R. O. Pimentel, J. I. Soletti, S. H. V. Carvalho, and L. Meili, "Biodiesel production from Sterculia striata oil by ethyl transesterification methodfication method," *Industrial Crops and Products*, vol. 74, pp. 767–772, 2015.

[17] D. A. Kamel, H. A. Farag, N. K. Amin, A. A. Zatout, and R. M. Ali, "Smart utilization of jatropha (*Jatropha curcas* Linnaeus) seeds for biodiesel production: optimization and mechanism," *Industrial Crops and Products*, vol. 111, pp. 407–413, 2018.

[18] E. Modiba, P. Osifo, and H. Rutto, "Biodiesel production from baobab (*Adansonia digitata* L.) seed kernel oil and its fuel properties," *Industrial Crops and Products*, vol. 59, pp. 50–54, 2014.

[19] H. L. Rutto and C. C. Enweremadu, "Optimization of production variables of biodiesel from manketti using response surface methodology," *International Journal of Green Energy*, vol. 8, no. 7, pp. 768–779, 2011.

[20] L. Wang and B. Li, "Properties of manchurian apricot (*Prunus mandshurica* Skv.) and siberian apricot (*Prunus sibirica* L.) seed kernel oils and evaluation as biodiesel feedstocks," *Industrial Crops and Products*, vol. 50, pp. 838–843, 2013.

[21] H. Durak, "Pyrolysis of xanthium strumariumin a fixed bed reactor: effects of boron catalysts and pyrolysis parameters on product yields and character," *Energy Sources, Part A: Recovery, Utilization, and Environmental Effects*, vol. 38, no. 10, pp. 1400–1409, 2016.

[22] E. Yücedağ and H. Durak, "Bio-oil and bio-char from lactuca scariola: significance of catalyst and temperature for assessing yield and quality of pyrolysis," *Energy Sources Part A Recovery Utilization and Environmental Effects*, pp. 1–14, 2019.

[23] H. Durak, S. Genel, and M. Tunç, "Pyrolysis of black cumin seed: significance of catalyst and temperature product yields and chromatographic characterization," *Journal of Liquid Chromatography and Related Technologies*, vol. 42, pp. 1–20, 2019.

[24] J. Fu, X. W. Zhang, K. Liu, Q. S. Li, L. R. Zhang, and X. H. Yang, "Hypolipidemic activity in sprague–dawley rats and constituents of a novel natural vegetable oil from cornus wilsoniana fruits," *Journal of Food Science*, vol. 77, no. 8, pp. 160–169, 2012.

[25] L. Lin, H. Cui, S. Vittayapadung et al., "Synthesis of KF/CaO as a catalyst for the production of bio-fuel from cracking of cornus wisonianaoil," *European Journal of Lipid Science and Technology*, vol. 117, no. 3, pp. 406–410, 2015.

[26] Y. Li, X. Wang, J. Chen et al., "A method for micropropagation of *cornus wilsoniana*: an important biofuel plant," *Industrial Crops and Products*, vol. 76, pp. 49–54, 2015.

[27] Y. Li, A. H. Zhang, Z. H. Xiao, C. Z. Li, and H. M. Wang, "Optimization of catalytic cracking conditions for *cornus wilsoniana* oil using V_2O_5/diatomite catalyst by response surface method," *Petrochemical Technology*, vol. 44, no. 7, pp. 882–887, 2015.

[28] A. H. Zhang, Z. H. Xiao, L. B. Zhang, and C. Z. Li, "Preparation of rich hydrocarbon fuels from *Swida wilsoniana* oil by coupling catalytic cracking and alcohol esterification," *Advances in New and Renewable Energy*, vol. 2, no. 5, pp. 342–346, 2014.

[29] A. Lankoff, K. Brzoska, J. Czarnocka et al., "A comparative analysis of in vitro toxicity of diesel exhaust particles from combustion of 1st-and 2nd-generation biodiesel fuels in relation to their physicochemical properties-the fuel health project," *Environmental Science and Pollution Research*, vol. 24, no. 23, pp. 19357–19374, 2017.

[30] M. Qasim, T. M. Ansari, and M. Hussain, "Experimental investigations on a diesel engine operated with fuel blends derived from a mixture of pakistani waste tyre oil and waste soybean oil biodiesel," *Environmental Science and Pollution Research*, vol. 25, no. 24, pp. 23657–23666, 2018.

[31] U. Derya, B. Nezahat, I. Oguzhan, and H. Nilufer, "Improvement of fuel properties of biodiesel with bioadditive ethyl levulinate," *Open Chemistry*, vol. 16, no. 1, pp. 647–652, 2018.

[32] Y. Wu, *Research on Hydro-Deoxygenation of Biodiesel to Produce Hydrocarbon Liquid Fuel*, Zhejiang University of Technology, Hangzhou, China, 2018.

[33] Q. Ouyang, J. W. Yao, J. Huang, N. Yang, and X. J. Liu, "Catalytic hydrodeoxygenation of fatty acid methyl esters over Pt/Al_2O_3-beta to produce second-generation biodiesel," *Petrochemical Technology*, vol. 47, no. 9, pp. 929–935, 2018.

[34] H. L. Zuo, Q. Y. Liu, T. J. Wang, N. Shi, J. G. Liu, and L. L. Ma, "Catalytic hydrodeoxygenation of vegetable oil over Ni catalysts to produce second-generation biodiesel," *Journal of Fuel Chemistry and Technology*, vol. 40, no. 9, pp. 1067–1073, 2012.

[35] K. Dhanalaxm, R. Singuru, S. Mondal et al., "Magnetic nanohybrid decorated porous organic polymer: synergistic catalyst for high performance levulinic acid hydrogenation," *ACS Sustainable Chemistry & Engineering*, vol. 5, no. 1, pp. 1033–1045, 2017.

[36] S. Mondal, R. Singuru, S. Chandra Shit et al., "Ruthenium nanoparticle-decorated porous organic network for direct hydrodeoxygenation of long-chain fatty acids to alkanes," *ACS Sustainable Chemistry & Engineering*, vol. 6, no. 2, pp. 1610–1619, 2018.

[37] H. Wang, S. Yan, S. O. Salley, and K. Y. S. Ng, "Hydrocarbon fuels production from hydrocracking of soybean oil using transition metal carbides and nitrides supported on ZSM-5," *Industrial & Engineering Chemistry Research*, vol. 51, no. 30, pp. 10066–10073, 2012.

[38] F. Wang, J. M. Xu, J. C. Jiang, P. Liu, M. H. Zhou, and K. Wang, "Advance in catalysts applied to bio-diesel production from oil hydrotreatment," *Materials Review*, vol. 32, no. 5, pp. 765–771, 2018.

[39] Q. Zhang, L. Zhang, D. Z. Zou et al., "Numerical simulation of reaction kettle and optimization of reaction conditions for soybean oil hydrogenation," *Food Science*, vol. 38, no. 6, pp. 253–260, 2017.

[40] S. Y. Han, X. H. Liu, and N. Z. Jiang, "Controlled synthesis of ZSM-5 molecular sieves with special morphologies," *Materials Review*, vol. 30, no. 6, pp. 111–130, 2016.

[41] D. P. Gamliel, G. M. Bollas, and J. A. Valla, "Bifunctional Ni-ZSM-5 catalysts for the pyrolysis and hydropyrolysis of biomass," *Energy Technology*, vol. 5, no. 1, pp. 172–182, 2016.